

Rapidity and Pseudorapidity distributions of the Various Hadron-Species Produced in High Energy Nuclear Collisions : A Systematic Approach

Goutam Sau^{1*}, A. Bhattacharya^{2†} & S. Bhattacharyya^{3‡}

¹ Beramara RamChandrapur High School,
South 24-Pgs, 743609(WB), India.

² Department of Physics,
Jadavpur University, Kolkata- 700032, India.

³ Physics and Applied Mathematics Unit(PAMU),
Indian Statistical Institute, Kolkata - 700108, India.

Abstract

With the help of a phenomenological approach outlined in the text in some detail, we have dealt here with the description of the plots on rapidity and pseudorapidity spectra of some hadron-secondaries produced in various nucleus-nucleus interactions at high energies. The agreement between the measured data and the attempted fits are, on the whole, modestly satisfactory excepting a very narrow central region in the vicinity of $y=\eta=0$. At last, hints to how the steps suggested in the main body of the text to proceed with the description of the measured data given in the plots could lead finally to a somewhat systematic methodology have also been made.

Keywords: Relativistic heavy ion collisions; inclusive cross-section; Inclusive production with identified hadrons; Quarks, gluons, and QCD in nuclear reactions.

PACS nos.:25.75.-q, 13.60.Hb, 13.85.Ni, 24.85.+p

*e-mail: sau-goutam@yahoo.com

†e-mail: pampa@phys.jdvu.ac.in

‡e-mail: bsubrata@www.isical.ac.in (Communicating Author).

1 Introduction and Background

In a chain of our previous works we studied extensively the properties of the rapidity (pseudorapidity) spectra of the various secondary particles in some very high energy collisions. The left-overs of the available latest data on rapidity (pseudorapidity) spectra would here be dealt with for some specific secondaries produced in some very high energy nuclear collisions. The secondary species studied herein are mostly clearly identified particles. Our objective here is quite clear. In the light of a Grand Combinational Model (GCM) we would dwell here upon some aspects of the behaviour of the rapidity (pseudorapidity) spectra of the identified secondaries produced in high energy Au+Au and Pb+Pb interactions. This would provide us an opportunity to check up the role of Grand Combinational Model (GCM) in explaining some very recent and interesting data on Au+Au and Pb+Pb reactions.

Amidst the two previous works, this paper is more in line with our second work[1] on understanding the nature of the rapidity spectra for production of some heavy baryons than with the first one. In this paper, an empirical energy-dependence of one of the parameters was introduced and a systematic approach to the study was built up. This work is just a follow-up of that particular methodology. This work is essentially just an exhaustive study on the rapidity-density or pseudorapidity-density of the identified hadronic secondaries produced in some high energy nuclear collisions. This apart, some clues to developing this procedure as a systematic approach have also been highlighted.

The paper is organized as follows. In the next section (Sec.2) we give the basic outlook and the approach to be taken up for this study. The following section (Sec.3) provides description of the data analyses on Au+Au and Pb+Pb interactions mostly in the graphical plots. The last section is reserved for summing up the conclusions with some suggestive remarks to develop the applied procedure into a somewhat complete systematic methodology.

2 The Phenomenological Setting : Premises and the Pathway

Following Faessler[2], Peitzmann[3], Schmidt and Schukraft[4] and finally Thomé et al[5], we [6, 7] had formulated in the past a final working expression for rapidity distributions in proton-proton collisions at ISR (Intersecting Storage Rings) ranges of energy-values by the following three-parameter

parametrization, viz,

$$\frac{1}{\sigma} \frac{d\sigma}{dy} = C_1 (1 + \exp \frac{y - y_0}{\Delta})^{-1} \quad (1)$$

where C_1 is a normalization constant and y_0 , Δ are two parameters. The choice of the above form made by Thomé et al[5] was intended to describe conveniently the central plateau and the fall-off in the fragmentation region by means of the parameters y_0 and Δ respectively. Besides, this was based on the concept of both limiting fragmentation and the Feynman Scaling hypothesis. For all five energies in PP collisions the value of Δ was obtained to be ~ 0.55 for pions[6] and kaons[7], ~ 0.35 for protons/antiprotons[7], and ~ 0.70 for Λ , Ξ , ϕ , Σ and Ω . And these values of Δ are generally assumed to remain the same in the ISR ranges of energy. Still, for very high energies, and for direct fragmentation processes which are quite feasible in very high energy heavy nucleus-nucleus collisions, such parameter values do change somewhat prominently, though in most cases with marginal high energies, we have treated them as nearly constant.

Now, the fits for the rapidity (pseudorapidity) spectra for non-pion secondaries produced in the PP reactions at various energies are phenomenologically obtained by De and Bhattacharyya[7] through the making of suitable choices of C_1 and y_0 . It is observed that for most of the secondaries the values of y_0 do not remain exactly constant and show up some degree of species-dependence . However, for Λ , Ξ , Σ , Ω and ϕ , it gradually increases with energies and the energy-dependence of y_0 is empirically proposed to be expressed by the following relationship[6] :

$$y_0 = k \ln \sqrt{s_{NN}} + 0.8 \quad (2)$$

The nature of energy-dependence of y_0 is shown in the adjoining figure (Fig.1). Admittedly, as k is assumed to vary very slowly with c. m. energy, the parameter y_0 is not exactly linearly correlated to $\ln \sqrt{s_{NN}}$, especially in the relatively low energy region. And this is clearly manifested in Fig.1. This variation with energy in k -values is introduced in order to accommodate and describe the symmetry in the plots on the rapidity spectra around mid-rapidity. This is just phenomenologically observed by us, though we cannot readily provide any physical justification for such perception and/or observation. And the energy-dependence of y_0 is studied here just for gaining insights in their nature and for purposes of extrapolation to the various higher energies (in the centre of mass frame, $\sqrt{s_{NN}}$) for several nucleon-nucleon, nucleon-nucleus and nucleus-nucleus collisions. The specific energy (in the c.m. system, $\sqrt{s_{NN}}$) for every nucleon-nucleus or nucleus-nucleus collision is first worked out by converting the laboratory energy value(s) in the required c.m. frame energy value(s). Thereafter

the value of y_0 to be used for computations of inclusive cross-sections of nucleon-nucleon collisions at particular energies of interactions is extracted from Eq. (2) for corresponding obtained energies. This procedural step is followed for calculating the rapidity (pseudorapidity)-spectra for not only the pions produced in nucleon-nucleus and nucleus-nucleus collisions[6]. However, for the studies on the rapidity-spectra of the non-pion secondaries produced in the same reactions one does always neither have the opportunity to take recourse to such a systematic step, nor could they actually resort to this rigorous procedure, due to the lack of necessary and systematic data on them.

Our next step is to explore the nature of $f(y)$ which is envisaged to be given generally by a polynomial form noted below :

$$f(y) = \alpha + \beta y + \gamma y^2, \quad (3)$$

where α , β and γ are the coefficients to be chosen separately for each AB collisions (and also for AA collisions when the projectile and the target are same). Besides, some other points are to be made here. The suggested choice of form in expression (3) is not altogether fortuitous. In fact, we got the clue from one of the previous work by one of the authors (SB)[8] here pertaining to the studies on the behavior of the EMC effect related to the lepto-nuclear collisions. In the recent past Hwa et al[9] also made use of this sort of relation in a somewhat different context. Now let us revert to our original discussion and to the final working formula for $\frac{dN}{dy}$ in various AB (or AA) collisions given by the following relation :

$$\frac{dN}{dy}|_{AB \rightarrow QX} = C_2(AB)^{\alpha + \beta y + \gamma y^2} \frac{dN}{dy}|_{PP \rightarrow QX} = C_3(AB)^{\beta y + \gamma y^2} (1 + \exp \frac{y - y_0}{\Delta})^{-1}, \quad (4)$$

where C_2 is the normalization constant and $C_3 = C_2(AB)^\alpha$ is another constant as α is also a constant for a specific collision at a specific energy. The parameter values for different nucleus-nucleus collisions are given in the Tables (Table2 - Table 11).

However, it is to be noted that the relationship between rapidity and pseudorapidity is given by the following standard relation

$$\frac{dN}{d\eta dp_T^2} = \sqrt{1 - \frac{m^2}{m_T^2 \cosh^2 y}} \frac{dN}{dy dp_T^2} \quad (5)$$

with the following properties :

- (a) In the region $y \gg 0$, $\frac{dN}{d\eta} \approx \frac{dN}{dy}$
- (b) But, in the region $y \rightarrow 0$, there is a small depression of the $\frac{dN}{d\eta}$ distribution relative to $\frac{dN}{dy}$ due to the above transformation. In experiments at high energies where $\frac{dN}{dy}$ has a plateau shape, this

transformation gives a small dip in $\frac{dN}{d\eta}$ around $\eta \approx 0$.

(c) In the c.m. frame, the peak of the distribution is located around $y \approx \eta \approx 0$, and the peak value of $\frac{dN}{d\eta}$ is smaller than the peak value of $\frac{dN}{dy}$; And this Diminutive Fraction Factor (DFF) is given by

$$DFF \approx [1 - \frac{m^2}{\langle m_T^2 \rangle}]^{\frac{1}{2}} \quad (6)$$

3 Depicting the Results Obtained

3.1 A Few Pointed Steps

The procedural steps for arriving at the results could be summed up as follows :

(i) We assume that the inclusive cross section (I.C.) of any particle in a nucleus-nucleus (AB) collision can be obtained from the production of the same in nucleon-nucleon collisions by multiplying the inclusive cross-section (I.C.) by a product of the atomic numbers of each of the colliding nuclei raised to a particular function, which is initially unspecified[10].

(ii) Secondly, we accept the property of factorization[1] of that particular function which helps us to perform the integral over p_T in a relatively simpler manner.

(iii) Thirdly, we assume a particular 3-parameter form for the pp cross section with the parameters C_1 , y_0 and Δ .

(iv) Finally, we accept the ansatz that the function $f(y)$ can be modeled by a quadratic function with the parameters α , β and γ .

3.2 Final Results Delivered

The results are shown here by the graphical plots with the accompanying tables for the parameter values. Here we draw the rapidity-density of pion(π), kaon(K), proton-antiproton(N), ϕ , Ω , Σ , Λ , Ξ for symmetric Pb+Pb and Au+Au collisions and pseudorapidity-density of charged-particle (mainly π^+) for symmetric Au+Au collisions at several energies which have been appropriately labeled at the top right corner. In this context some comments are in order. Though the figures represents the case for production of pion(π), kaon(K), proton-antiproton(N), ϕ , Ω , Σ , Λ , Ξ , we do not anticipate and/or expect any strong charge-dependence of the results. Besides, the solid curves in all cases-almost without any exception-demonstrate our GCM-based results. Secondly, the data on rapidity(pseudorapidity)-spectra for some high-energy collisions are, at times, available for both

positive and negative $y(\eta)$ -values. This gives rise to a problem in our method. It is evident here in this work that we are concerned with only symmetric collisions wherein the colliding nuclei must be identical. But in our expression (4) the coefficient β multiplies a term which is proportional to y and so is not symmetric under $y \rightarrow (-y)$. In order to overcome this difficulty we would introduce here $\beta=0$ for all the graphical plots (except Fig.12). These plots are represented by Fig.2 to Fig.11 for $\pi, K, \phi, N, \Sigma, \Xi, \Lambda, \Omega$ in Pb+Pb and Au+Au collision under different conditions. The parameter values in this particular case are presented in tables (Table 2 - Table 10). The graphical plots shown in fig.2 and Fig.3 (for $\beta=0$) are for production of π^-, K^-, K^+, ϕ in Pb+Pb collisions at 20A GeV, 30A GeV, 40A GeV, 80A GeV respectively. The diagrams shown in Fig.4 represent the production of $\pi, N, K, \Sigma, \Lambda, \Xi, \Omega$ in Au+Au interaction at $\sqrt{s(NN)}=7$ GeV (for $\beta=0$). And the plots depicted for pseudorapidity-spectra in Fig.5 to Fig.11 are based on the production of charged particle (we consider only π^+) in Au+Au collision for different centrality bins at 19.6 GeV, 62.4 GeV, 130 GeV and 200 GeV respectively (for $\beta=0$). The plots shown in Fig.12 are for the production of charged particle (mainly π^+) for four different energies i.e., 19.6 GeV, 62.4 GeV, 130 GeV, 200 GeV respectively and the parameter values are shown in Table 11. Here we would mention that the data are for 19.6 GeV, 130 GeV, 200 GeV for PHOBOS Collaboration and that of 62.4 GeV for STAR Collaboration as shown on the top right corner of the figure. Finally, the diagram in Fig.13 represents the variation of β and γ with the energy values and we draw a mean curve in this particular diagram.

4 Concluding Remarks and Some Comments

On an overall basis, our model-based results are in fair agreement with the most of the data-sets, excepting $y \approx 0$ or $\eta \approx 0$ region, wherein the data shows flat-plateau structures in almost all the diagrams exhibiting data on both positive and negative rapidities or pseudorapidities. The degree of disagreement in the vicinity of $\eta \approx 0$ region is evidently much stronger for the plots on pseudorapidity-density versus pseudorapidity plots. These discrepancies might probably be ascribed to our simplistic assumption of $y=\eta$. Had we been able to compute the diminutive fraction factor (DFF) as given by expression (6), we would have been capable of giving the pseudorapidity-figures much better looks. And this computation is not possible because of the fact that the rapidity-data-sets do not generally offer even the slightest hints on the p_T -ranges of the secondaries under

observations and/or measurements.

The last figure of this paper carries some special physical significance which we now explain below. This is, by essence, undoubtedly a purely phenomenological model with no or very little predictive capacity. The energy-dependences studied in Fig. 13 for some of the involved parameters, β and γ , could provide us some insights into what could be the possible values of β and γ at some higher/lower/intermediate values of the c.m. energies of the interactions for any specific secondary. This could help, we believe, to reduce the elements/components of phenomenology and introduce some degree, however low, of predictivity of values of β and γ by necessary intrapolation or extrapolation, as the case may be, for any specific secondary produced in the same nuclear interactions. Thus, if sufficient and reliable data at, at least, six to seven c.m. energies at reasonable intervals are available allowing the scopes for studying the nature of c.m. energy-dependence of these parameters, the present procedure could be nurtured to a better and more competent methodical approach.

References

- [1] Goutam Sau, P.Guptaroy, A.C.Das Ghosh and S.Bhattacharyya, *Il Nuovo Cimento* **B** 2010 125(11) 1379.
- [2] M.A.Faessler, *Phys. Rep.*, 1984 115(1 & 2) 1.
- [3] T.Peitzmann, *Phys. Lett.* **B**, 1999 450(1-3) 7.
- [4] H.R.Schmidt and J.Schukraft, *J. Phys.* **G**, 1993 19(11) 1705.
- [5] W.Thomé et al, *Nucl. Phys.* **B** 1977 129(3) 365.
- [6] B.De, S.Bhattacharyya and P.Guptaroy, *Int. J. Mod. Phys.* **A** 2002 17(30) 4615.
- [7] B.De and S.Bhattacharyya, *Int. J. Mod. Phys.* **A** 2004 19(14) 2313.
- [8] S.Bhattacharyya, *Lett. Nuovo Cimento* 1985 42(2) 119.
- [9] R.C.Hwa et al, *Phys. Rev.* **C** 2001 64(5) 054611.
- [10] Goutam Sau, S.K.Biswas, A.C.Das Ghosh, A.Bhattacharya and S.Bhattacharyya, *Il Nuovo Cimento* **B** 2010 125(7) 833.
- [11] SUN Le-Xue et al, *Chinese Phys.* **C** 2009 33(10) 1 hep-ph/1105.0577 v1 03 May 2011.
- [12] Lie-Wen Chen et al., *nucl-th/1103.0916* v1 04 March 2011.
- [13] B. Alver et al (PHOBOS Collaboration), *Phys. Rev.* **C** 2011 83(2) 024913.
- [14] J.Adams et al (STAR Collaboration), *Phys. Rev.* **C** 2006 73(3) 034906.

Table 1: Variation of y_0 with Energy.[Reference Fig. No.1]

$Energy(\sqrt{s_{NN}})(GeV)$	$Constant(k)$	y_0
6.3(20 AGeV)	2.76	5.894
7	2.65	5.951
7.6(30 AGeV)	2.54	6.006
8.7(40 AGeV)	2.40	6.085
12.3(80 AGeV)	2.16	6.276
19.6	1.92	6.517
62.4	1.54	7.153
130	1.39	7.556
200	1.32	7.794

Table 2: Values of different parameters for production of identified hadrons in central Pb+Pb collisions at $E_{beam} = 20$ AGeV (for $\beta=0$) for both +ve and -ve rapidities.[Reference Fig. No.2(a) & 3(a)]

$Production$	C_3	γ	$\frac{\chi^2}{ndf}$
π^-	84.941 ± 0.2108	-0.044 ± 0.0003	21.509/22
K^+	20.574 ± 0.1556	-0.057 ± 0.0008	4.119/05
K^-	05.507 ± 0.0447	-0.091 ± 0.0015	7.753/14
ϕ	01.325 ± 0.0406	-0.139 ± 0.0021	4.423/07

Table 3: Values of different parameters for production of identified hadrons in central Pb+Pb collisions at $E_{beam} = 30$ AGeV (for $\beta=0$) for both +ve and -ve rapidities.[Reference Fig. No.2(b) & 3(b)]

$Production$	C_3	γ	$\frac{\chi^2}{ndf}$
π^-	97.912 ± 0.2754	-0.037 ± 0.0003	10.898/13
K^+	22.849 ± 0.1128	-0.049 ± 0.0005	5.824/08
K^-	07.547 ± 0.0705	-0.075 ± 0.0011	4.316/10
ϕ	01.384 ± 0.0158	-0.095 ± 0.0008	4.264/06

Table 4: Values of different parameters for production of identified hadrons in central Pb+Pb collisions at $E_{beam} = 40$ AGeV (for $\beta=0$) for both +ve and -ve rapidities.[Reference Fig. No.2(c) & 3(c)]

$Production$	C_3	γ	$\frac{\chi^2}{ndf}$
π^-	111.998 ± 0.3811	-0.035 ± 0.0003	8.926/10
K^+	023.363 ± 0.1275	-0.039 ± 0.0005	4.621/06
K^-	010.605 ± 0.0755	-0.073 ± 0.0003	3.394/09
ϕ	001.185 ± 0.0147	-0.063 ± 0.0006	4.206/09

Table 5: Values of different parameters for production of identified hadrons in central Pb+Pb collisions at $E_{beam} = 80$ AGeV (for $\beta=0$) for both +ve and -ve rapidities.[Reference Fig. No.2(d) & 3(d)]

<i>Production</i>	C_3	γ	$\frac{\chi^2}{ndf}$
π^-	147.686 ± 0.4383	-0.027 ± 0.0002	8.659/11
K^+	026.426 ± 0.1038	-0.030 ± 0.0004	5.455/08
K^-	012.790 ± 0.0763	-0.041 ± 0.0007	9.002/12
ϕ	001.762 ± 0.0044	-0.044 ± 0.0002	0.543/06

Table 6: Values of different parameters for production of identified hadrons in central Au+Au collisions at $\sqrt{s_{NN}} = 7$ GeV (for $\beta=0$) for both +ve and -ve rapidities.[Reference Fig. No.4]

<i>Production</i>	C_3	γ	$\frac{\chi^2}{ndf}$
π	299.742 ± 0.4296	-0.026 ± 0.0001	8.014/07
N	136.702 ± 0.2569	-0.048 ± 0.0005	5.460/04
K	011.734 ± 0.0248	-0.030 ± 0.0001	0.621/03
Σ, Λ	015.886 ± 0.0055	-0.056 ± 0.0004	4.750/05
Ω	000.017 ± 0.0004	-0.079 ± 0.0048	8.754/10
Ξ	000.628 ± 0.0037	-0.057 ± 0.0010	9.502/14

Table 7: Values of different parameters for production of charged-particle (π^+) in Au+Au collisions at $\sqrt{s_{NN}} = 19.6$ GeV (for $\beta=0$) for both +ve and -ve pseudo-rapidities.[Reference Fig. No.5]

<i>Centrality</i>	C_3	γ	$\frac{\chi^2}{ndf}$
03% – 06%	363.098 ± 1.764	-0.0157 ± 0.00009	17.359/12
06% – 10%	328.094 ± 1.195	-0.0148 ± 0.00007	12.873/19
10% – 15%	266.638 ± 0.967	-0.0137 ± 0.00007	21.209/18
15% – 20%	207.392 ± 1.130	-0.0125 ± 0.00008	9.160/10
20% – 25%	180.106 ± 0.656	-0.0123 ± 0.00007	15.549/16
25% – 30%	150.634 ± 0.456	-0.0117 ± 0.00006	14.747/12
30% – 35%	115.939 ± 0.436	-0.0110 ± 0.00007	16.130/15
35% – 40%	087.982 ± 0.405	-0.0098 ± 0.00008	11.447/13
40% – 45%	071.793 ± 0.249	-0.0093 ± 0.00008	16.840/10

Table 8: Values of different parameters for production of charged-particle (π^+) in Au+Au collisions at $\sqrt{s_{NN}} = 62.4$ GeV (for $\beta=0$) for both +ve and -ve pseudo-rapidities.[Reference Fig. No.6 & 7]

<i>Centrality</i>	C_3	γ	$\frac{\chi^2}{ndf}$
00% – 03%	858.977 ± 2.349	-0.0131 ± 0.00002	3.527/04
03% – 06%	805.167 ± 1.252	-0.0135 ± 0.00008	9.541/12
06% – 10%	690.250 ± 4.553	-0.0126 ± 0.00006	15.843/13
10% – 15%	505.765 ± 2.056	-0.0111 ± 0.00004	15.882/15
15% – 20%	397.679 ± 1.516	-0.0101 ± 0.00004	11.527/12
20% – 25%	288.758 ± 1.128	-0.0086 ± 0.00005	9.042/10
25% – 30%	223.869 ± 1.019	-0.0081 ± 0.00004	8.544/08
30% – 35%	179.875 ± 0.496	-0.0076 ± 0.00004	10.873/11
35% – 40%	126.863 ± 0.661	-0.0066 ± 0.00005	10.169/10
40% – 45%	112.144 ± 0.404	-0.0068 ± 0.00005	6.154/05
45% – 50%	091.802 ± 0.290	-0.0077 ± 0.00004	11.346/09

Table 9: Values of different parameters for production of charged-particle (π^+) in Au+Au collisions at $\sqrt{s_{NN}} = 130$ GeV (for $\beta=0$) for both +ve and -ve pseudo-rapidities.[Reference Fig. No.8 & 9]

Centrality	C_3	γ	$\frac{\chi^2}{ndf}$
00% – 03%	1017.26 ± 4.767	-0.0106 ± 0.00006	8.489/08
03% – 06%	859.123 ± 4.007	-0.0096 ± 0.00005	11.504/11
06% – 10%	771.332 ± 4.214	-0.0094 ± 0.00005	11.448/11
10% – 15%	553.134 ± 1.895	-0.0083 ± 0.00002	11.348/07
15% – 20%	490.218 ± 2.056	-0.0084 ± 0.00004	13.212/15
20% – 25%	384.377 ± 1.812	-0.0079 ± 0.00004	9.556/16
25% – 30%	342.650 ± 1.736	-0.0081 ± 0.00004	14.193/13
30% – 35%	264.987 ± 1.080	-0.0077 ± 0.00004	8.711/13
35% – 40%	183.701 ± 0.757	-0.0061 ± 0.00005	3.271/06
40% – 45%	165.105 ± 0.243	-0.0068 ± 0.00001	11.067/08
45% – 50%	115.942 ± 0.417	-0.0065 ± 0.00003	8.366/13

Table 10: Values of different parameters for production of charged-particle (π^+) in Au+Au collisions at $\sqrt{s_{NN}} = 200$ GeV (for $\beta=0$) for both +ve and -ve pseudo-rapidities.[Reference Fig. No.10 & 11]

Centrality	C_3	γ	$\frac{\chi^2}{ndf}$
00% – 03%	1305.84 ± 6.334	-0.0095 ± 0.00004	8.374/07
03% – 06%	1217.02 ± 3.923	-0.0092 ± 0.00002	2.677/07
06% – 10%	1085.85 ± 5.787	-0.0089 ± 0.00003	8.494/08
10% – 15%	786.155 ± 5.756	-0.0083 ± 0.00004	10.695/07
15% – 20%	671.544 ± 0.816	-0.0080 ± 0.00001	13.220/08
20% – 25%	494.043 ± 4.083	-0.0076 ± 0.00005	8.479/08
25% – 30%	371.719 ± 2.104	-0.0069 ± 0.00004	7.826/06
30% – 35%	298.854 ± 2.012	-0.0069 ± 0.00005	10.232/07
35% – 40%	298.430 ± 1.067	-0.0077 ± 0.00001	19.517/16
40% – 45%	142.160 ± 0.609	-0.0060 ± 0.00003	11.112/10
45% – 50%	203.956 ± 0.874	-0.0063 ± 0.00003	13.112/08

Table 11: Values of different parameters for production of charged-particle (π^+) in Au+Au collisions at four different energies for +ve pseudo-rapiditie only.[Reference Fig. No.12]

Energy(GeV)	C_3	β	γ	$\frac{\chi^2}{ndf}$
19.6	361.238 ± 3.900	0.015 ± 0.00032	-0.020 ± 0.00009	8.596/25
62.4	778.667 ± 8.000	0.018 ± 0.00028	-0.018 ± 0.00008	3.847/04
130	511.297 ± 7.890	0.027 ± 0.00054	-0.012 ± 0.00015	14.445/25
200	557.934 ± 7.087	0.028 ± 0.00044	-0.011 ± 0.00011	9.578/26

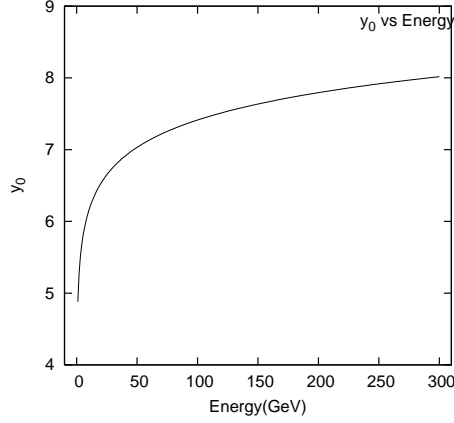


Figure 1: Variation of y_0 in equation (2) with increasing energy.[Parameter values are shown in Table 1.]

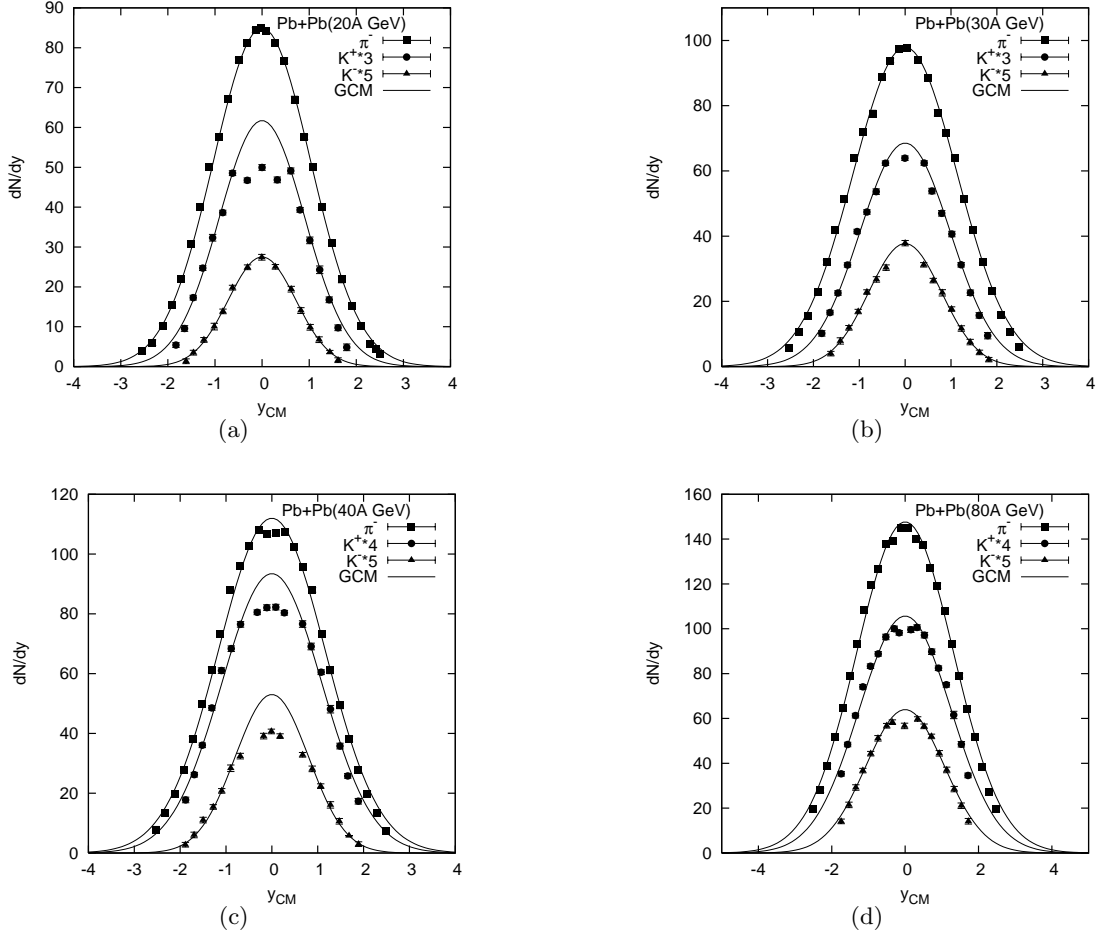


Figure 2: Rapidity distributions of identified hadrons in central Pb+Pb collisions at $E_{beam} = 20, 30, 40, 80$ AGeV for $\beta=0$. The symbols are the experimental data and the data points are taken from [11] and the parameter values are taken from Table 2-Table 5. The solid curve provide the GCM-based results.

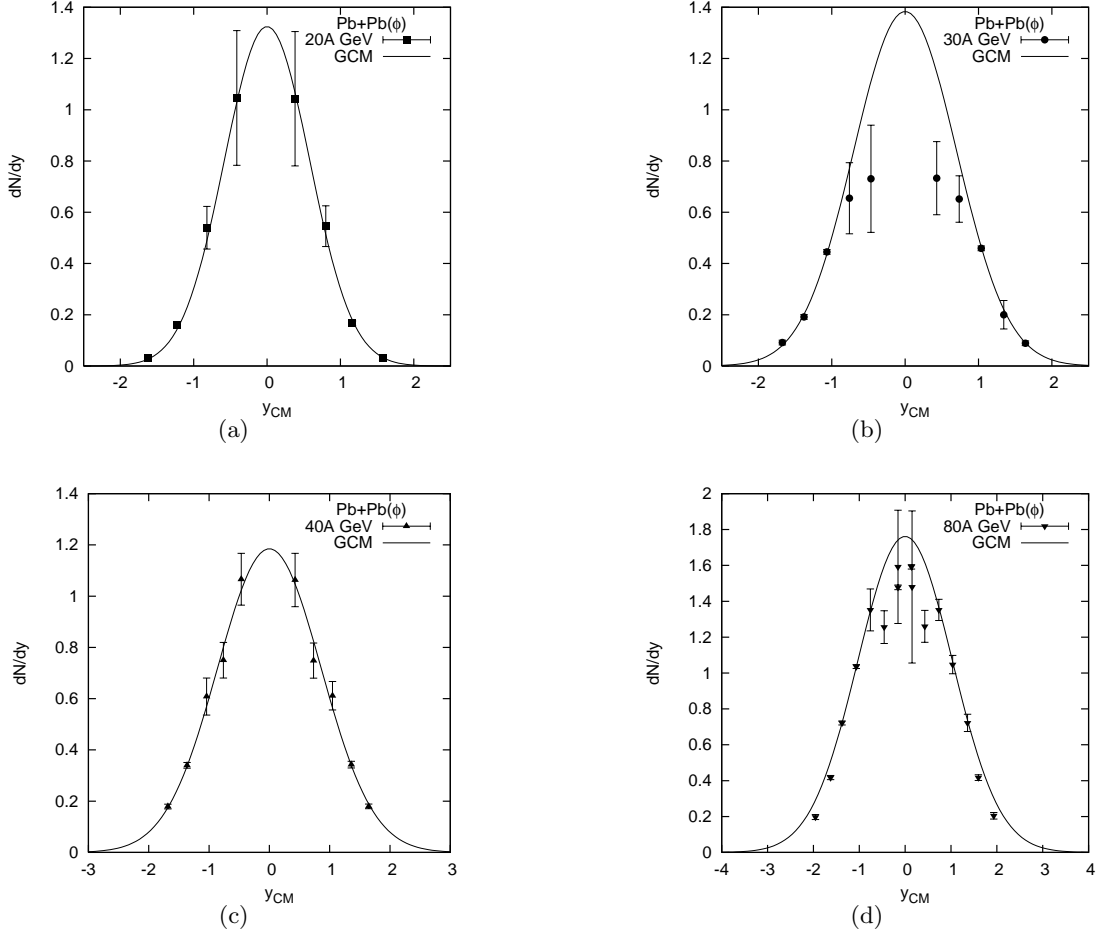


Figure 3: Rapidity spectra for ϕ in central Pb+Pb collisions at $E_{beam} = 20, 30, 40, 80$ AGeV for $\beta=0$. The different experimental points are taken from [11] and the parameter values are taken from Table 2-Table 5. The solid curve provide the GCM-based results.

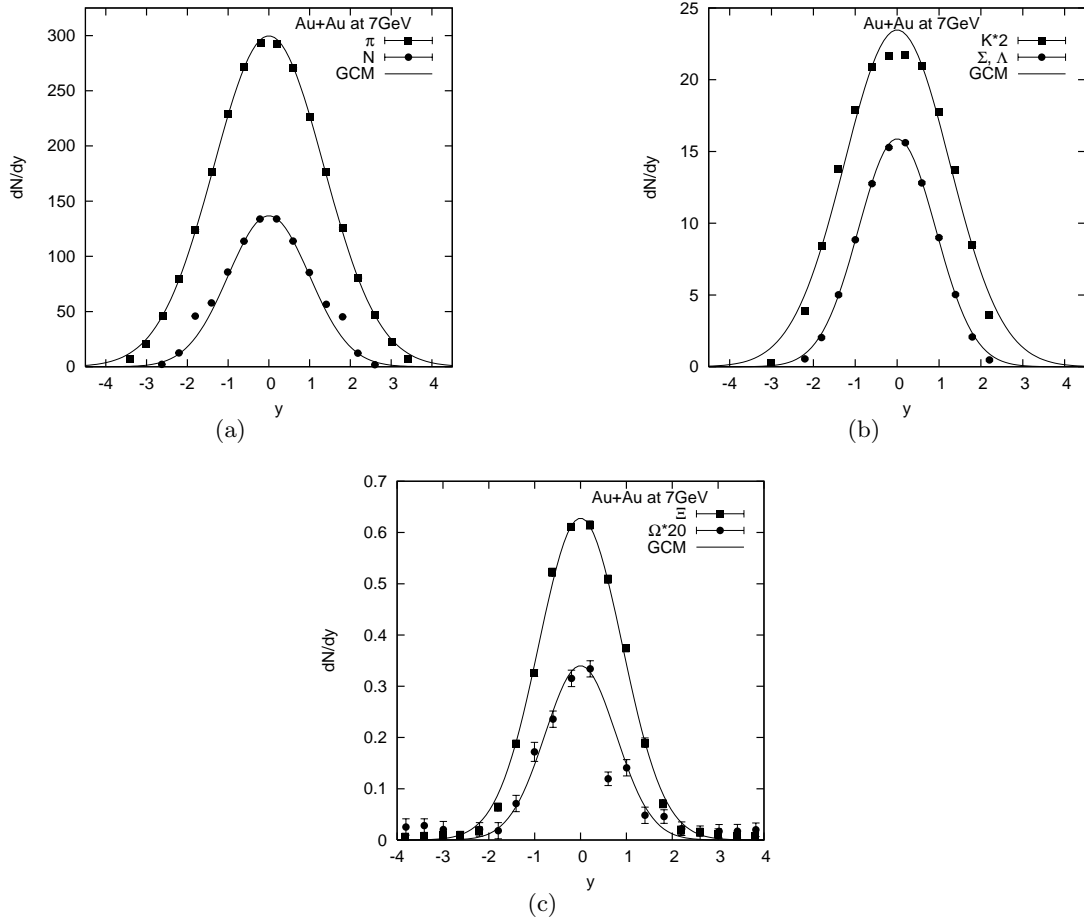


Figure 4: Rapidity distributions of identified hadrons in central Au+Au collisions at $\sqrt{s_{NN}} = 7$ GeV for $\beta = 0$. The different experimental points are taken from [12] and the parameter values are taken from Table 6. The solid curve provide the GCM-based results.

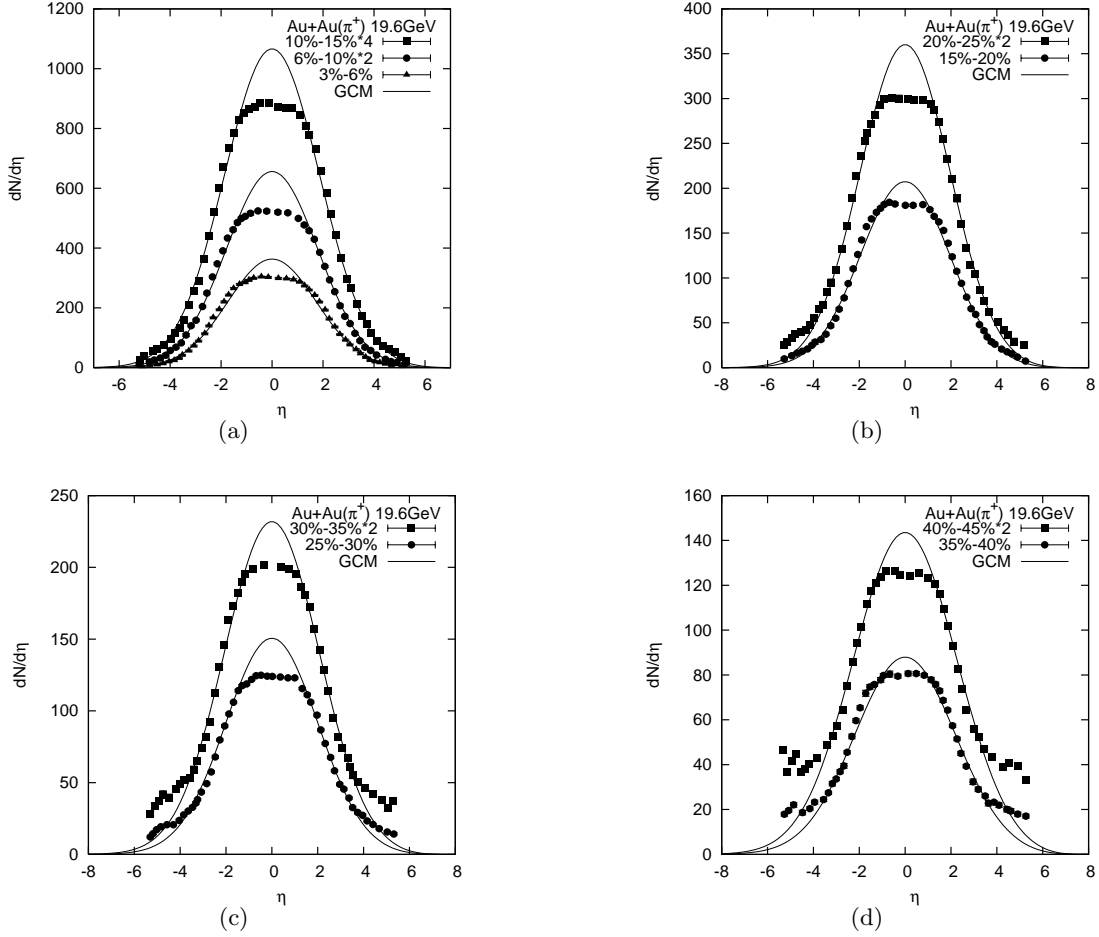


Figure 5: Pseudo-rapidity spectra for π^+ for nine centrality bins representing 45% of the total cross-section for Au+Au collisions at $\sqrt{s_{NN}}=19.6$ GeV for $\beta=0$. The different experimental points are taken from [13] and the parameter values are taken from Table 7. The solid curve provide the GCM-based results.

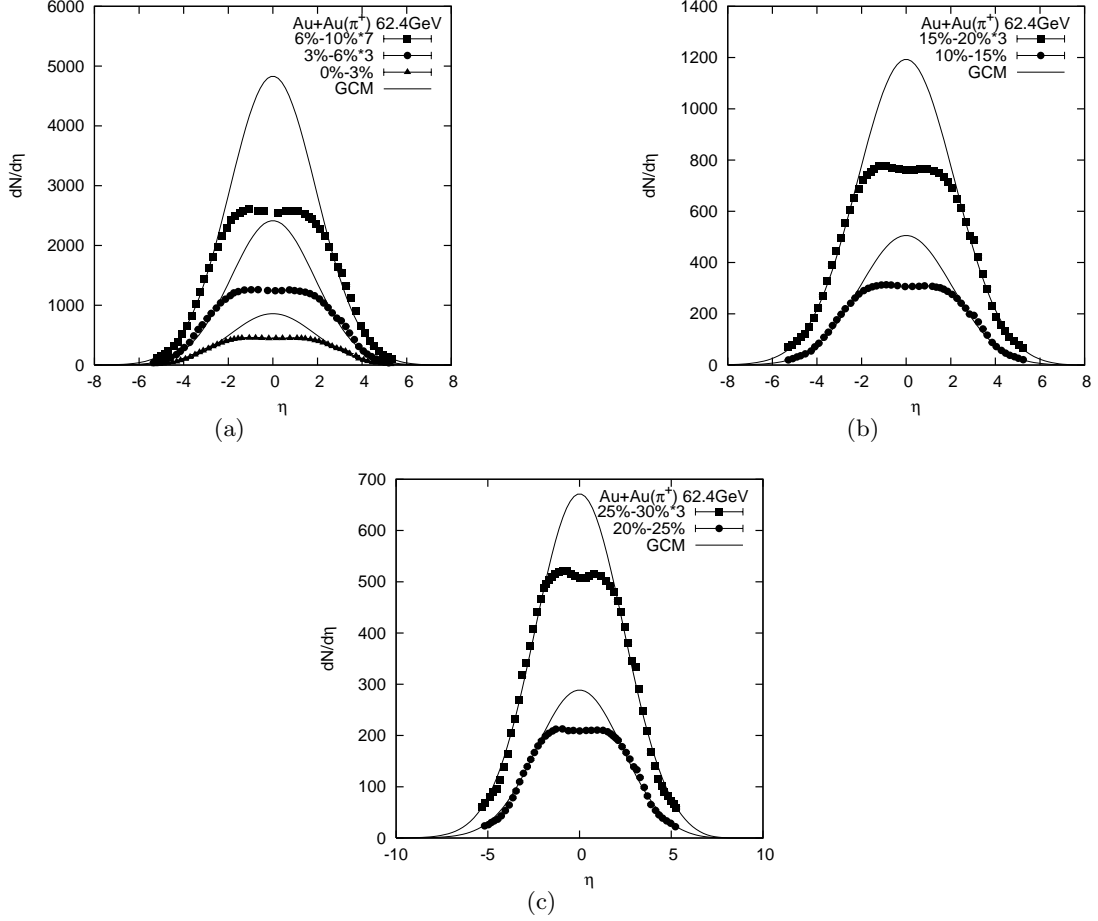


Figure 6: Plot of $\frac{dN}{d\eta}$ vs. η for π^+ for seven centrality bins representing 45% of the total cross-section for Au+Au collisions at $\sqrt{s_{NN}} = 62.4$ GeV for $\beta = 0$. The different experimental points are taken from [13] and the parameter values are taken from Table 8. The solid curve provide the GCM-based results.

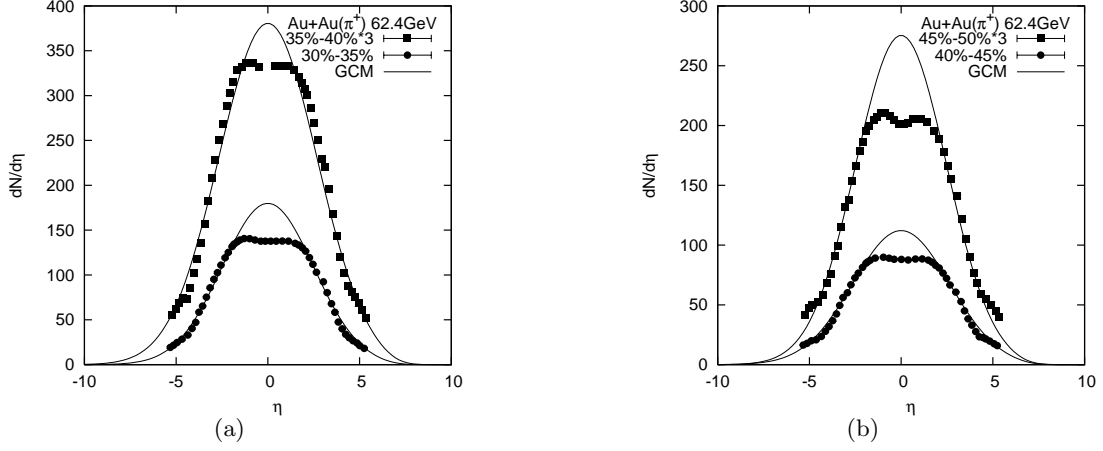


Figure 7: Plot of $\frac{dN}{d\eta}$ vs. η for π^+ for four centrality bins representing 45% of the total cross-section for Au+Au collisions at $\sqrt{s_{NN}}=62.4$ GeV for $\beta=0$. The different experimental points are taken from [13] and the parameter values are taken from Table 8. The solid curve provide the GCM-based results.

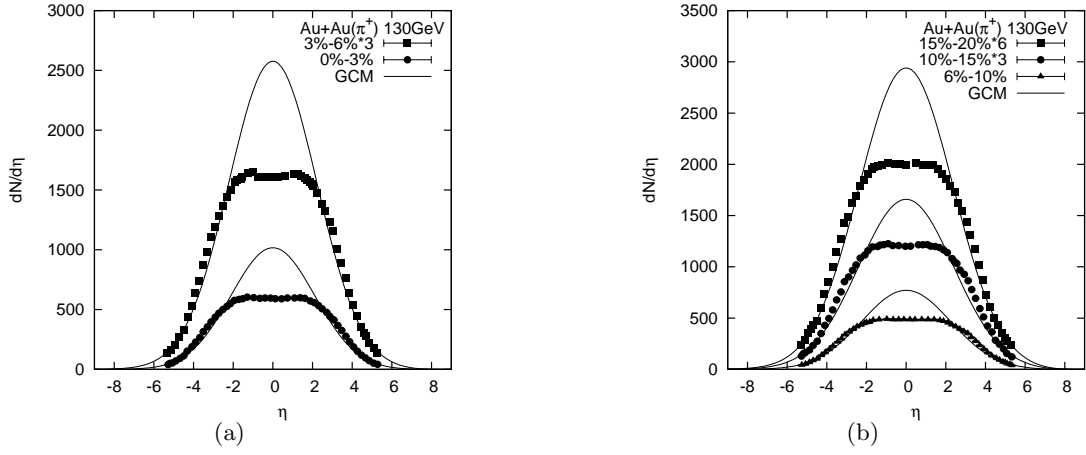


Figure 8: Pseudo-rapidity spectra for π^+ for five centrality bins representing 45% of the total cross-section for Au+Au collisions at $\sqrt{s_{NN}}=130$ GeV for $\beta=0$. The different experimental points are taken from [13] and the parameter values are taken from Table 9. The solid curve provide the GCM-based results.

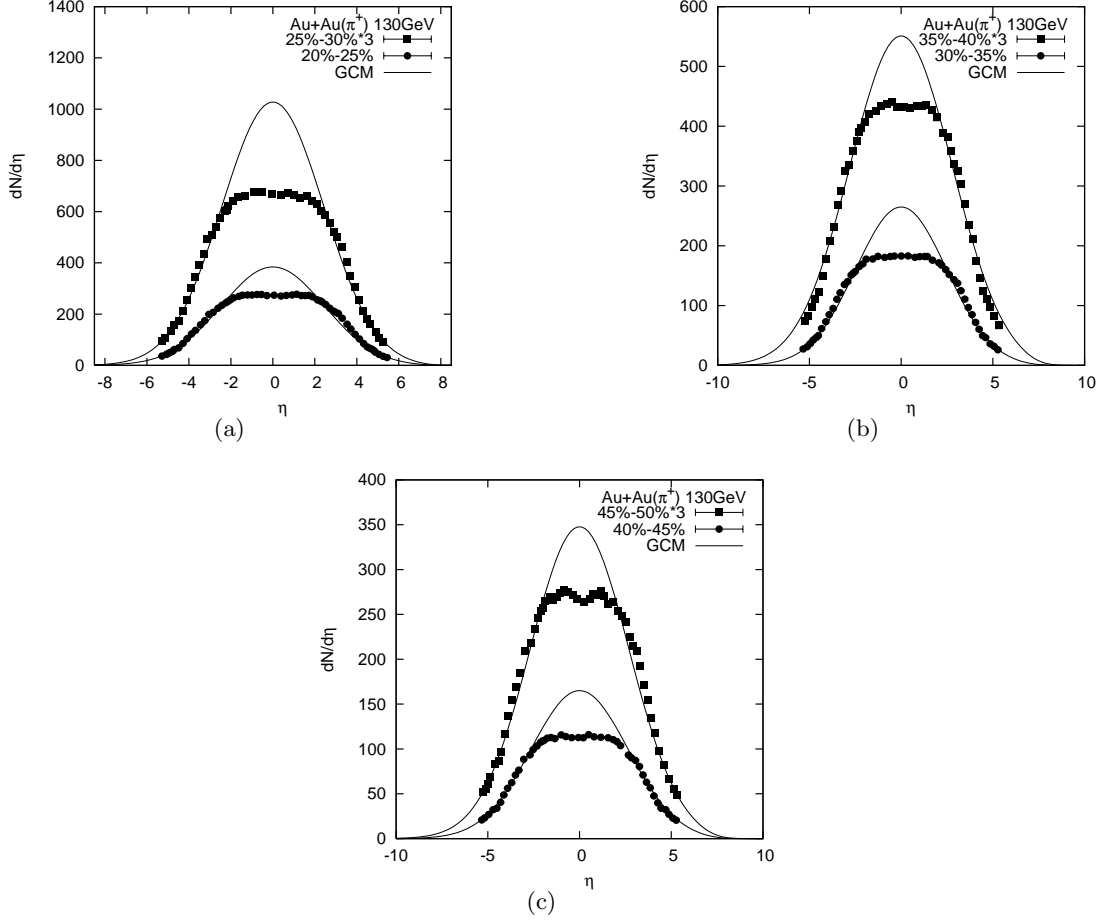


Figure 9: Pseudo-rapidity spectra for π^+ for six centrality bins representing 45% of the total cross-section for Au+Au collisions at $\sqrt{s_{NN}}=130$ GeV for $\beta=0$. The different experimental points are taken from [13] and the parameter values are taken from Table 9. The solid curve provide the GCM-based results.

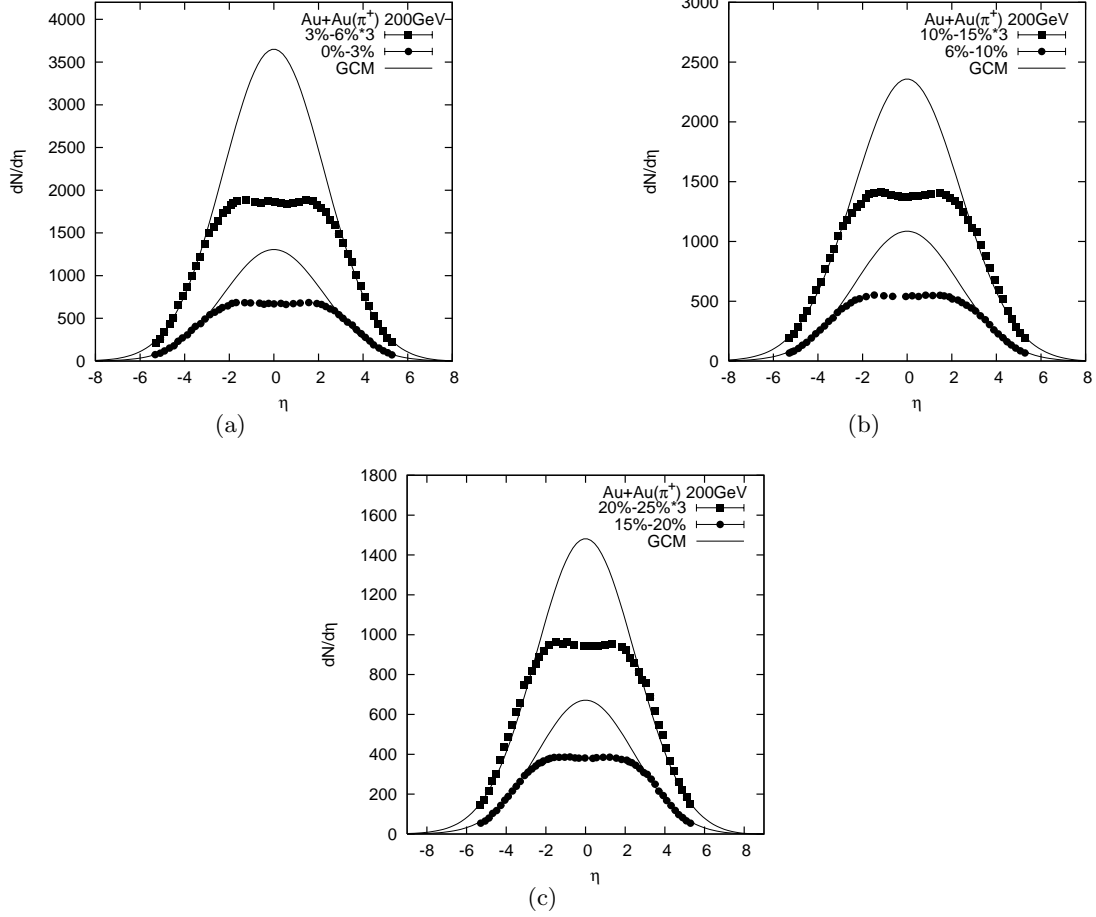


Figure 10: Plot of $\frac{dN}{d\eta}$ vs. η for π^+ for six centrality bins representing 45% of the total cross-section for Au+Au collisions at $\sqrt{s_{NN}}=200$ GeV for $\beta=0$. The different experimental points are taken from [13] and the parameter values are taken from Table 10. The solid curve provide the GCM-based results.

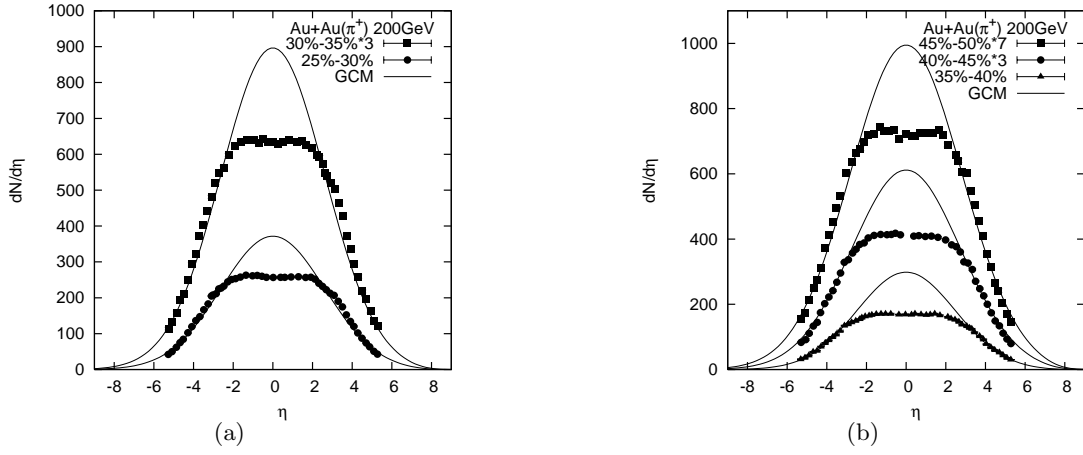


Figure 11: Plot of $\frac{dN}{d\eta}$ vs. η for π^+ for five centrality bins representing 45% of the total cross-section for Au+Au collisions at $\sqrt{s_{NN}}=200$ GeV for $\beta=0$. The different experimental points are taken from [13] and the parameter values are taken from Table 10. The solid curve provide the GCM-based results.

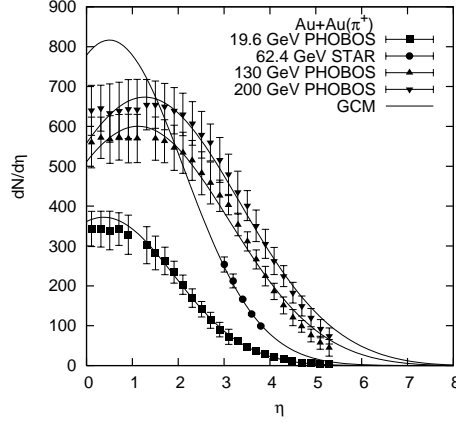


Figure 12: Pseudorapidity distributions of charged particles(for π^+) for various c.m. energies in Au+Au central collisions. Pseudorapidity distributions for 0-6% central Au+Au collisions at $\sqrt{s_{NN}} = 200, 130,$ and 19.6 GeV are from the PHOBOS experiment and 62.4 GeV is from STAR experiment($\beta \neq 0$). The different experimental points are taken from [14] and the parameter values are taken from Table 11 . The solid curve provide the GCM-based results.

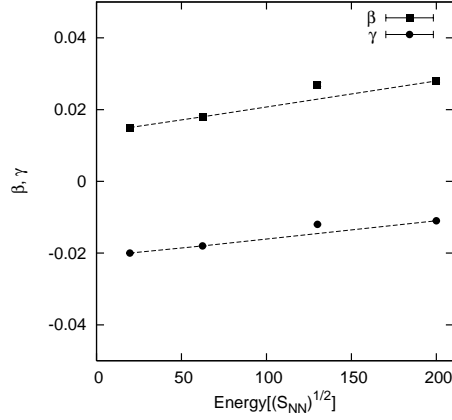


Figure 13: Variation of β and γ with increasing energy. All values are taken form Table 11.